Обзор ArXiv/astro-ph, 29 октября – 8 ноября 2024

От Сильченко О.К.

ArXiv: 2410.21370

An Indication of Gas Inflow in Clumpy Star-Forming Galaxies near $z \sim 1$: Lower Gas-Phase Metallicities in Clumpy Galaxies Compared to Non-Clumpy Galaxies

Visal Sok,[1] Adam Muzzin,[1] Pascale Jablonka,[2] Vivian Yun Yan Tan,[1] Z. Cemile Marsan,[1] Danilo Marchesini,[3] Gillian Wilson,[4] and Leo Y. Alcorn[5]

[1]*Department of Physics and Astronomy, York University, 4700 Keele St, Toronto, ON M3J 1P3, Canada*
[2]*Laboratoire d'astrophysique, École Polytechnique Fédérale de Lausanne (EPFL), CH-1290 Sauverny, Switzerland*
[3]*Department of Physics & Astronomy, Tufts University, 419 Boston Ave, Medford, MA 02155, USA*
[4]*Department of Physics, University of California Merced, 5200 Lake Road, Merced, CA 95343, USA*
[5]*David A. Dunlap Department of Astronomy & Astrophysics, University of Toronto, 50 Saint George Street, Toronto, ON M5S 3H4, Canada*

(Received January 25, 2024; Revised October 30, 2024)

ABSTRACT

Despite the ubiquity of clumpy star-forming galaxies at high-redshift, the origin of clumps are still largely unconstrained due to the limited observations that can validate the mechanisms for clump formation. We postulate that if clumps form due to the accretion of metal-poor gas that leads to violent disk instability, clumpy galaxies should have lower gas-phase metallicities compared to non-clumpy galaxies. In this work, we obtain the near-infrared spectrum for 42 clumpy and non-clumpy star-forming galaxies of similar masses, SFRs, and colors at $z \approx 0.7$ using the Gemini Near-Infrared Spectrograph (GNIRS) and infer their gas-phase metallicity from the [NII]λ6584 and Hα line ratio. We find that clumpy galaxies have lower metallicities compared to non-clumpy galaxies, with an offset in the weighted average metallicity of 0.07 ± 0.02 dex. We also find an offset of 0.06 ± 0.02 dex between clumpy and non-clumpy galaxies in a comparable sample of 23 star-forming galaxies at $z \approx 1.5$ using

Выборки:

- GNIRS: <z>=0.7 (32 галактики)
- FMOS/COSMOS: <z>=1.5 (23 галактики)
- Все галактики – их массы и темпы звездообразования – из обзора COSMOS/ULTRAVISTA (30 фотометрических полос, 0.15-24 мкм)

Using the stellar masses and SFRs from the UltraVISTA catalog, we then select galaxies of similar masses and SFRs to ensure that any observed metallicity offset is not driven by the fundamental metallicity relation. The masses were derived by fitting the spectral energy distribution of 30 photometric filters, extending from $0.15 - 24$ μm, and the SFRs were determined from the rest-frame UV and infrared luminosity. We select primarily galaxies with $\log(M_*/M_\odot) \approx 10.5$. This corresponds to star-forming galaxies with a high SFR ($\gtrsim$10 $M_\odot yr^{-1}$), and therefore increases the likelihood of a strong detection for both Hα and [NII]λ6584. Lastly, we select galaxies of similar colors (i.e., $U-V$ and $V-J$) to mitigate the effect of dust in our analyses as galaxies with higher dust attenuation generally have higher metallicities.

Figure 1 summarizes our GNIRS galaxy sample. We select 42 galaxies; 23 are clumpy galaxies and 19 are non-clumpy galaxies (the classification of clumpy and non-clumpy is presented in Section 2.4). **The solid markers denote galaxies that have a detection of** SNR > 3 **in both Hα and [NII]λ6584. Throughout the analysis we use only these S/N > 3 galaxies, which reduces our sample to 32 galaxies.** The average mass for the clumpy galaxies is $\log(M_*/M_\odot) = 10.48^{+0.15}_{-0.02}$, with an average SFR of $\log(\mathrm{SFR}\ [M_\odot\ yr^{-1}]) = 1.23^{+0.19}_{-0.14}$. The average mass for non-clumpy galaxies is $\log(M_*/M_\odot) = 10.54^{+0.04}_{-0.06}$, and their average SFR is $\log(\mathrm{SFR}\ [M_\odot\ yr^{-1}]) = 1.30^{+0.12}$

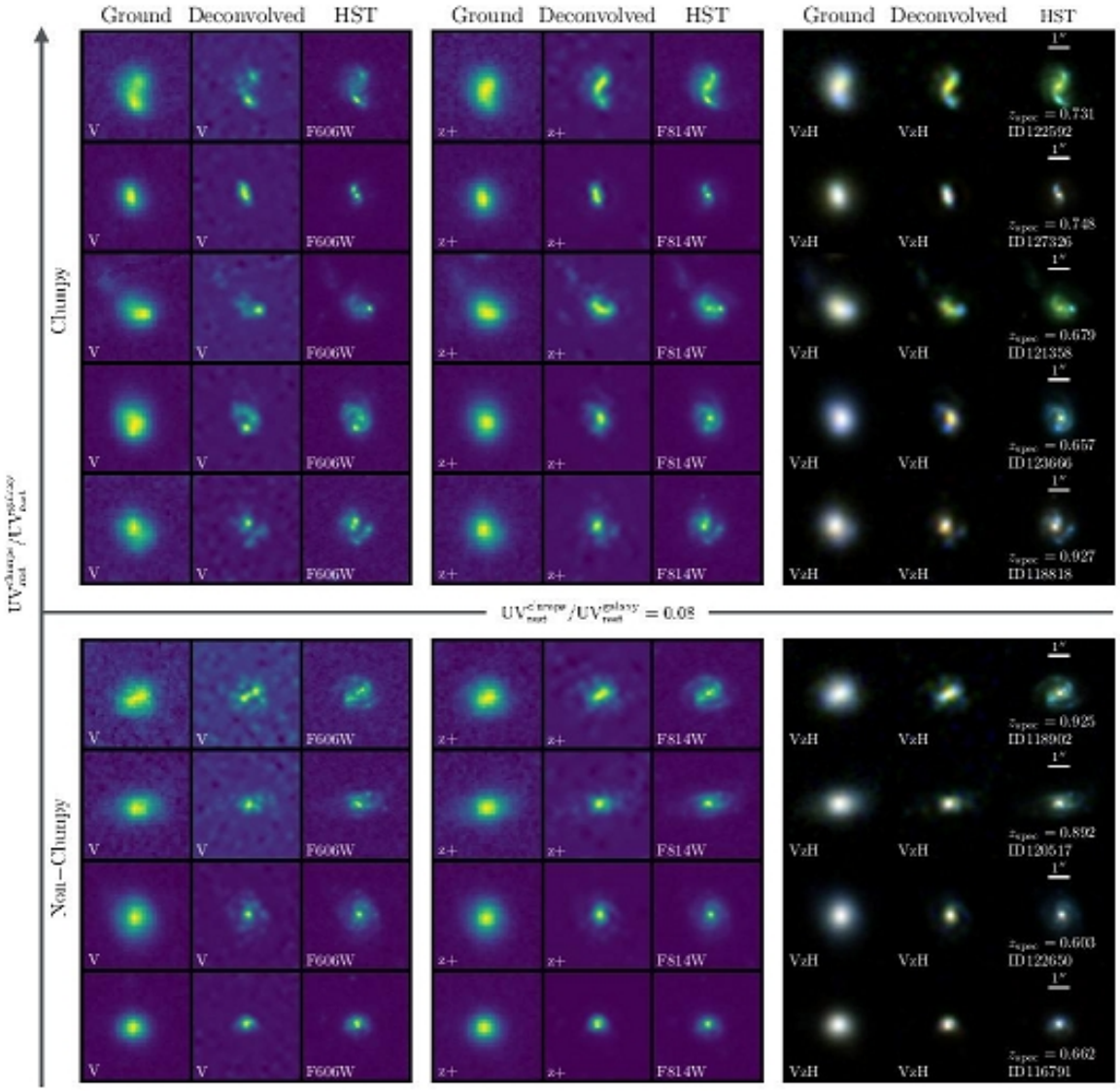

Figure 2. Comparison of deconvolved images to the corresponding HST images. From the left to right panel, we compare the *V*-band imaging to *F606W*, *z+*-band imaging to *F814W*, and the composite *VzH* image to a composite image constructed from *F606W*+*F814W*+*F160W*. Each stamp is $7.8'' \times 7.8''$. For each panel, the left to right column shows the ground-based image, the deconvolved image, and the corresponding HST image. Only 9 out of the 42 galaxies from our sample have HST imaging in the 3 HST filters. The images are deconvolved to a resolution of 0.3", corresponding to a physical scale of ∼2.3 kpc at $z \approx 0.7$. We arrange the figure such that the galaxies are shown in ascending order based on their clumpiness, as defined by the ratio of rest-frame UV light emitted from clumps relative to the host galaxy. Clumpy galaxies are those with clumps that have at least 8% of the total rest-frame UV luminosity.

Суммирование спектров вдоль щели с учетом скоростей

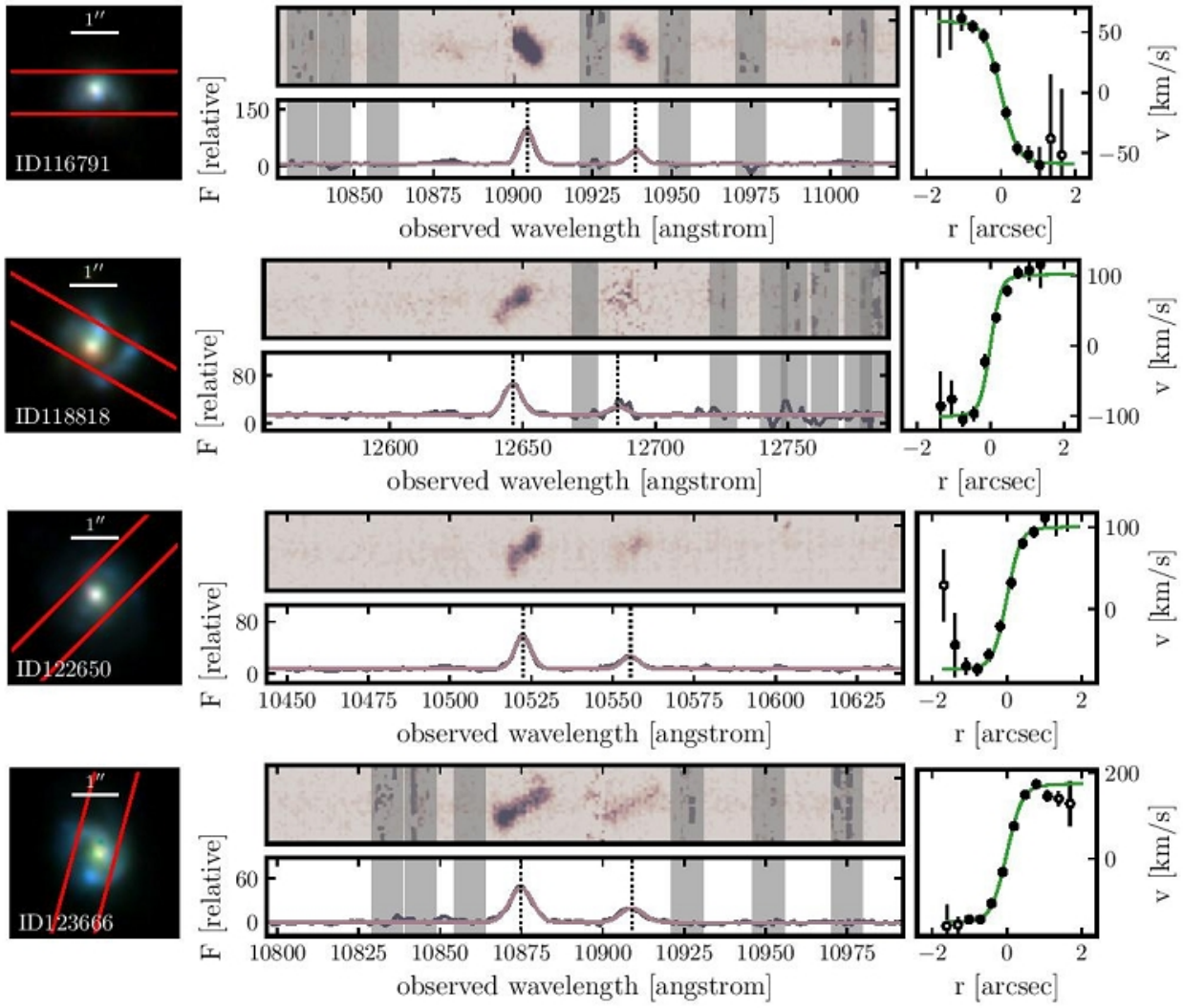

Пониженная металличность в галактиках со сгустками

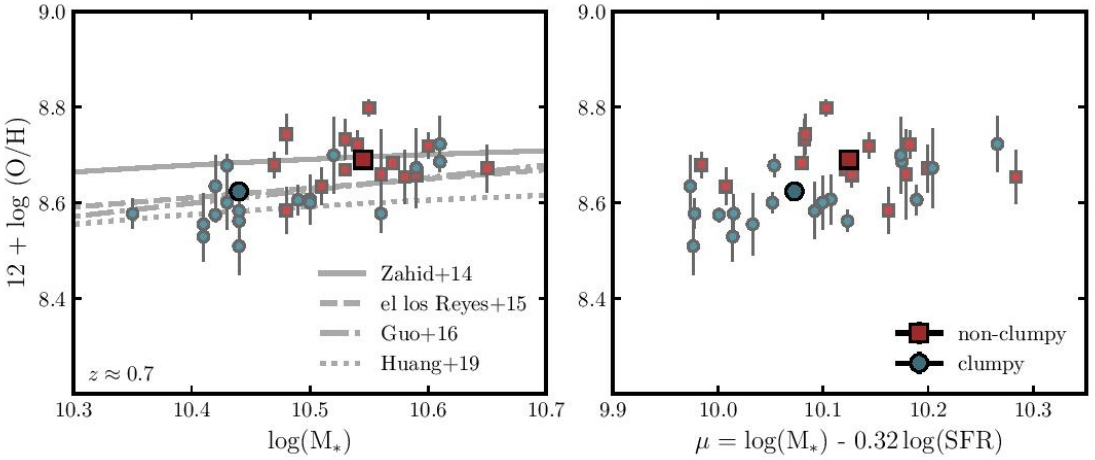

Figure 5. Left: the metallicities of clumpy and non-clumpy galaxies in relation to stellar masses. The dark, larger markers show the weighted average. The different lines show the mass-metallicity relation for galaxies at $z \approx 0.8$ from Zahid et al. (2014); de los Reyes et al. (2015); Guo et al. (2016), and Huang et al. (2019). The error is calculated as the weighted standard error. Right: The metallicities in relation to the projected stellar masses and star formation rate.

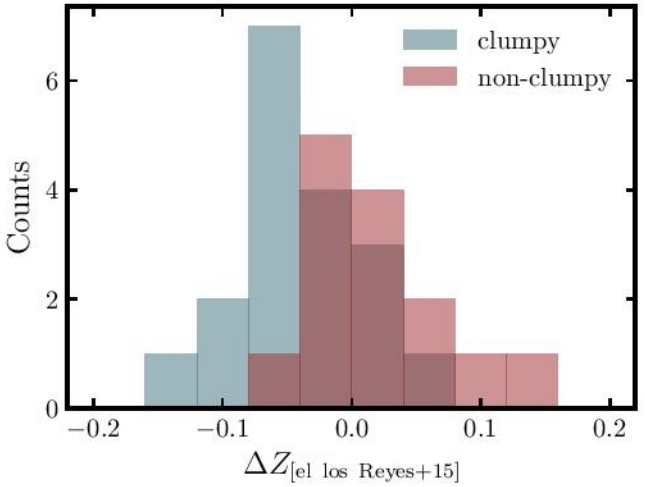

Figure 6. The histogram of the differences between the observed metallicity and the re-normalized mass-metallicity relation from de los Reyes et al. (2015) for clumpy and non-clumpy galaxies. Using a KS test, we find the two distributions are statistically different, with a p-value of 0.004.

То же самое и на z=1.5

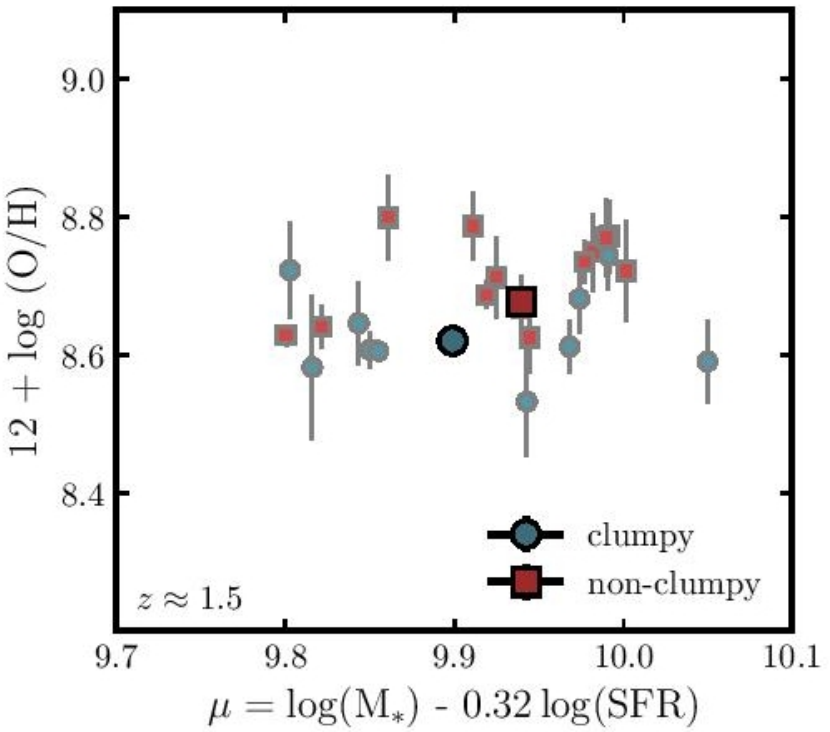

Figure 7. The fundamental metallicity relation of clumpy and non-clumpy galaxies in the FMOS-COSMOS sample. The darker markers shows the weighted average, and the error is taken as the weighted standard error. In general, the metallicity of clumpy and non-clumpy galaxies in the FMOS-COSMOS sample are similar to the GNIRS sample. The metallicity offset is measured to be 0.06 ± 0.02 dex.

Динамический анализ – так себе…

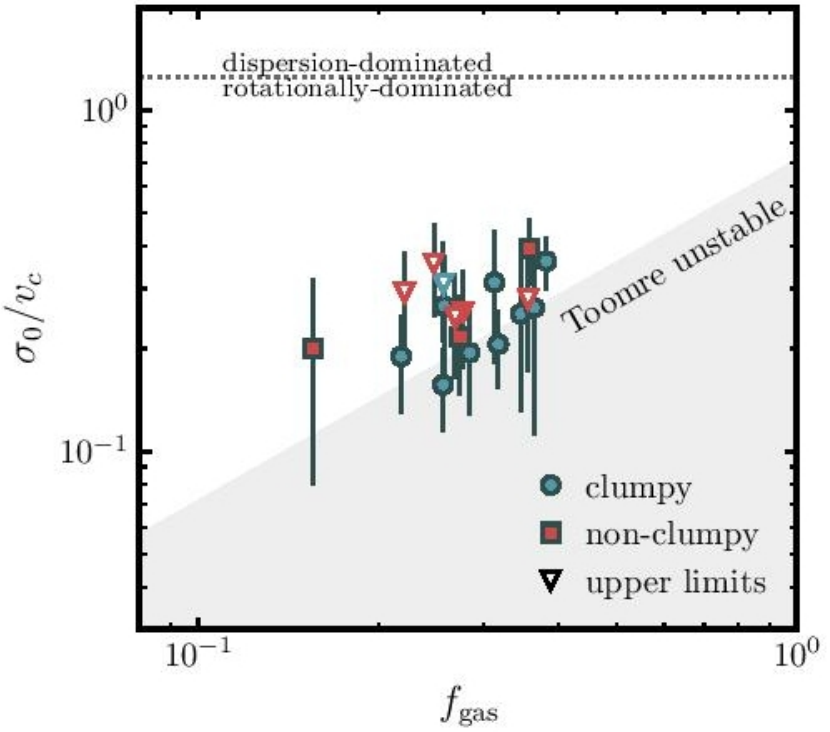

Figure 8. The relation between σ_0/v_c and $f_{\rm gas}$ for clumpy and non-clumpy galaxies. $f_{\rm gas}$ is derived from the integrated SFR, using the Kennicutt-Schmidt relation. The darker color markers show the mean value, and the error is calculated as the standard error of the mean. The dotted line shows the typical cutoff between rotationally- and dispersion-dominated systems Förster Schreiber et al. (2009). The shaded region shows the parameter space in which the Toomre Q value is less than 1 (i.e., unstable disks). This relation is defined by Eqn. 7 (see text for the deriva-

ArXiv: 2411.03593

ALMA detection of [OIII] 88 μm at $z = 12.33$: Exploring the Nature and Evolution of GHZ2 as a Massive Compact Stellar System

Jorge A. Zavala [1], Tom Bakx [2], Ikki Mitsuhashi [3], Marco Castellano [4], Antonello Calabro [4], Hollis Akins [5], Veronique Buat [6], Caitlin M. Casey [5], David Fernandez-Arenas [7,8], Maximilien Franco [5], Adriano Fontana [9], Bunyo Hatsukade [1,10,11], Luis C. Ho [12,13], Ryota Ikeda [1,14], Jeyhan Kartaltepe [15], Anton M. Koekemoer [16], Jed McKinney [17], Lorenzo Napolitano [18,19], Pablo G. Pérez-González [20], Paola Santini [21], Stephen Serjeant [22], Elena Terlevich [23,24,25], Roberto Terlevich [23,24,25] and L. Y. Aaron Yung [16]

[1] *National Astronomical Observatory of Japan, 2-21-1 Osawa, Mitaka, Tokyo 181-8588, Japan*

[2] *Department of Space, Earth, & Environment, Chalmers University of Technology, Chalmersplatsen 4 412 96 Gothenburg, Sweden*

[3] *Waseda Research Institute for Science and Engineering, Faculty of Science and Engineering, Waseda University, 3-4-1, Okubo, Shinjuku, Tokyo 169-8555, Japan*

[4] *INAF - Osservatorio Astronomico di Roma, via di Frascati 33, 00078 Monte Porzio Catone, Italy*

[5] *Department of Astronomy, The University of Texas at Austin, 2515 Speedway Boulevard Stop C1400, Austin, TX 78712, USA*

[6] *Aix Marseille Univ, CNRS, CNES, LAM, Marseille, France*

[7] *Canada-France-Hawaii Telescope, Kamuela, HI 96743, USA*

[8] *Instituto de Radioastronomía y Astrofísica, UNAM Campus Morelia, Apartado postal 3-72, 58090 Morelia, Michoacán, Mexico*

[9] *INAF - Osservatorio Astronomico di Roma, Via Frascati 33, 00078, Monte Porzio Catone, Italy*

[10] *Graduate Institute for Advanced Studies, SOKENDAI, Osawa, Mitaka, Tokyo 181-8588, Japan*

[11] *Institute of Astronomy, Graduate School of Science, The University of Tokyo, 2-21-1 Osawa, Mitaka, Tokyo 181-0015, Japan*

[12] *Kavli Institute for Astronomy and Astrophysics, Peking University, Beijing 100871, China*

[13] *Department of Astronomy, School of Physics, Peking University, Beijing 100871, China*

[14] *Department of Astronomy, School of Science, SOKENDAI (The Graduate University for Advanced Studies), 2-21-1 Osawa, Mitaka, Tokyo 181-8588, Japan*

[15] *Laboratory for Multiwavelength Astrophysics, School of Physics and Astronomy, Rochester Institute of Technology, 84 Lomb Memorial Drive, Rochester, NY 14623, USA*

[16] *Space Telescope Science Institute, 3700 San Martin Drive, Baltimore, MD 21218, USA*

[17] *Department of Astronomy, The University of Texas at Austin, 2515 Speedway Boulevard Stop C1400, Austin, TX 78712, USA*

[18] *INAF – Osservatorio Astronomico di Roma, via Frascati 33, 00078, Monteporzio Catone, Italy*

[19] *Dipartimento di Fisica, Università di Roma Sapienza, Città Universitaria di Roma - Sapienza, Piazzale Aldo Moro, 2, 00185, Roma, Italy*

Линия [OIII]88мкм видна уверенно; на 52 мкм – верхний предел

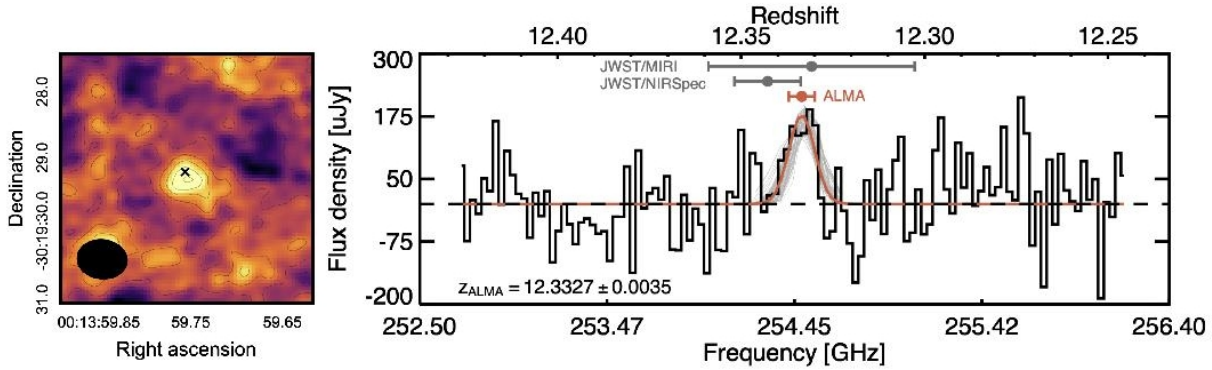

Figure 1. *Detection of the [OIII] 88 μm transition at $z = 12.3$.* The left panel shows the $3''.5 \times 3''.5$ moment-0 map of the line, along with the ALMA beam-size (black ellipse) and the JWST NIRCam position of GHZ2 (black cross). Contours show signal-to-noise ratio in steps of $\pm 1\sigma$ (with dashed lines for negative values). The $\sim 5\sigma$ detection from ALMA is in very good agreement with the JWST position. The extracted spectrum from the peak pixel is shown on the right panel along with the best-fit Gaussian function (red solid line) and associated uncertainty (gray lines; see main text for details), implying a spectroscopic redshift of $z = 12.3327 \pm 0.0035$. On the top, we show the associated redshifts inferred from the different instruments, including NIRSpec, MIRI, and ALMA. Thanks to the higher spectral resolution of the ALMA observations, the redshift precision is increased by $\sim 5\times$.

Table 1. [OIII] 88 μm line properties (uncorrected for gravitational amplification).

GHZ2	
RA = 00:13:59.76; Dec = −30:19:29.16	
$z_{[OIII]88\mu m}$	12.3327 ± 0.0035
$z_{NIRSpec}$ [a]	12.342 ± 0.009
z_{MIRI} [b]	12.33 ± 0.04
ν_{cent} [GHz]	254.487 ± 0.019
FWHM [km s^{-1}]	186 ± 58
S_{total} [mJy km s^{-1}]	36 ± 10
$L_{[OIII]}$ [$L_\odot$]$\times 10^8$	1.7 ± 0.4

[a] Castellano et al. (2024)

[b] Zavala et al. (2024)

Это звездообразование, а не AGN!

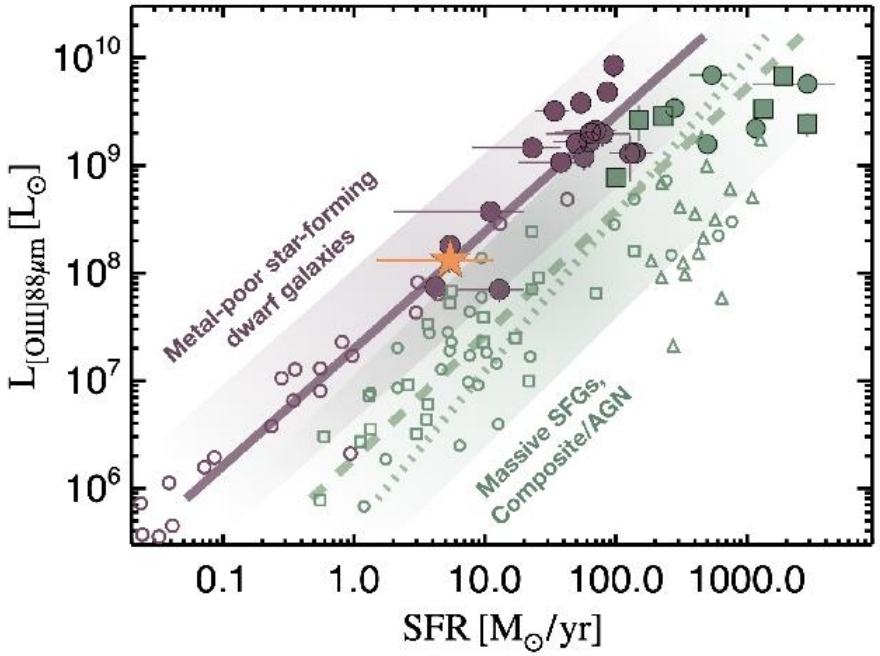

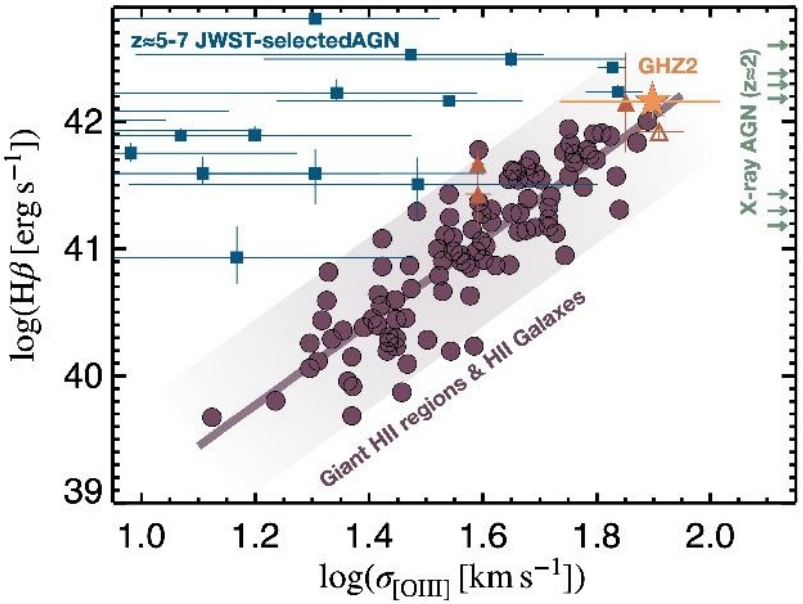

Нет темной материи!

Assuming a spherical geometry (a reasonable assumption for this very compact source), we estimate the dynamical mass using the virial equation (e.g. Pettini et al. 2001; Wolf et al. 2010):

$$M_{\rm dyn} = \frac{5\sigma^2 R}{G}, \quad (1)$$

where σ is the velocity dispersion and R is the virial radius. The velocity dispersion is determined from the [OIII] 88μm transition ($\sigma = 79 \pm 25\,{\rm km\,s^{-1}}$) and the virial radius is adopted to be the half-light radius measured from the JWST/NIRcam images, with reported values of $r_{1/2} = 39 \pm 11\,{\rm pc}$ (Ono et al. 2023) and $105 \pm 9\,{\rm pc}$ (Yang et al. 2022). Using Equation 1 and the aforementioned assumptions we constrain the dynamical mass to be $3 \times 10^8 - 8 \times 10^8\,{\rm M_\odot}$.

This is remarkably similar to the stellar masses inferred from the spectro-photometric SED fitting analysis presented in Zavala et al. (2024), with best-fit stellar masses of $2 \times 10^8 - 8 \times 10^8\,{\rm M_\odot}$ (assuming a magnification of $\mu = 1.3$: Bergamini et al. 2023). This implies a dynamical-to-stellar mass ratio of close to unity for GHZ2, similar to the measured values for globular clusters (e.g. Forbes et al. 2014), providing more evidence for a relation between these objects as discussed below.

Получится ли из GHZ2 шаровое скопление?

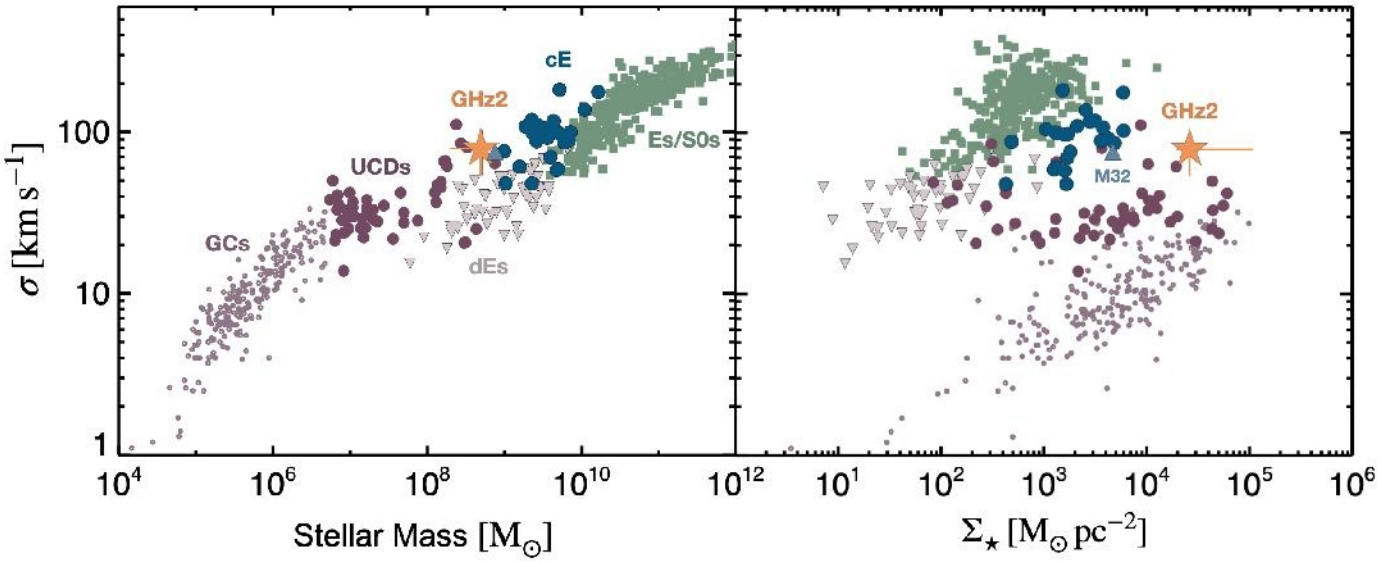

Figure 5. *The stellar mass-velocity dispersion relationship.* The velocity dispersion as a function of stellar mass (left) and stellar mass surface density (right) for different populations of pressure-supported systems (taken from Norris et al. 2014), including globular clusters (light purple circles), ultra-compact dwarfs (solid purple circles), dwarf ellipticals (down-pointing triangles), compact ellipticals (blue solid circles), and ellipitcal and S0 galaxies (green squares). Our target, GHZ2, represented by the yellow star, shows a similar stellar mass surface density as globular clusters, but with a higher total stellar mass that is in better agreement with those of ultra-compact dwarfs and compact ellipticals. Indeed, it occupies a similar locus as M32, the prototypical compact elliptical galaxy (represented by the up-pointing blue triangle). Note, however, that significant mass losses are expected due to stellar and dynamical evolution that would eventually affect the position of GHZ2 on this parameter space.